International Journal of Sciences: Basic and Applied Research (IJSBAR)

ISSN 2307-4531
(Print & Online)

https://gssrr.org/index.php/JournalOfBasicAndApplied/index

Development of ^{64}Cu-doped Gold Nanoparticles for In-vitro and In-vivo Studies

Solmaz Bastani [a]*, Elena Echeverria[b], Allison Roberts[c]

[a]*Physics Department, Oklahoma State University, 145 Physical Sciences II, Stillwater, OK 74078, USA (currently at Wofford College)*

[b]*Physics Department, Oklahoma State University, 145 Physical Sciences II, Stillwater, OK 74078, USA (currently at Cornell University)*

[c]*Department of Physics, Davidson College, Davidson, NC 28035, USA*

[a]*Email: bastanis@wofford.edu*

[b]*Email:eme54@cornell.edu*

[c]*Email:robertsallison@ufl.edu*

Abstract

Gold Nanoparticles (GNPs) have been utilized as radiosensitizers to amplify radiation's effect on specifically targeted cancerous cells. Since traditional GNPs are not inherently radioactive, it complicates the ability to measure their distribution and clearance from the body following administration to ensure that they are localized to the tumors rather than healthy tissue. In this study, novel GNPs were developed by doping the GNPs with ^{64}Cu. These GNPs were then characterized by ultraviolet-visible (UV-Vis) spectroscopy, Transmission Electron Microscopy (TEM), Energy Dispersive X-ray Spectroscopy (EDS), Inductively Coupled Plasma (ICP) emission spectroscopy, and X-ray Photoelectron Spectroscopy (XPS). Additionally, to compare the biocompatibility of ^{64}Cu@Au GNPs to that of traditional GNPs, in vitro cytotoxicity studies as well as in vivo biodistribution and pharmacokinetics studies were conducted. After measuring the viability of A-549 cells after exposure to varying concentrations of hybrid GNPs, the IC_{50} value measured falls within the expected range for traditional GNPs. Further, the hybrid GNPs were administered to mice samples, and the organs and tissues were collected at different time intervals and analyzed for radioactivity levels.

Received: *8/15/2024*
Accepted: *10/15/2024*
Published: *10/25/2024*

---

* Corresponding author.

The results showed that the organs most responsible for clearing the ^{64}Cu@Au GNPs from the blood were the liver, intestines, lungs, and kidneys, with a very low collection of the GNPs in the heart and brain. Furthermore, the pharmacokinetics clearances of the GNPs in these studies aligned with the expected clearance rates for various similarly sized biocompatible nanoparticles. Overall, these preliminary studies suggest that unfunctionalized ^{64}Cu@Au GNPs display biological properties and toxicity similar to those of traditional GNPs.

Keywords: Cancer Imaging; Gold Nanoparticles; Cytotoxicity; Biodistribution; Pharmacokinetics.

1. Introduction

Radiation therapy used to treat cancerous tumors can become less effective due to the likelihood of damaging healthy tissue compounded by the growing resistance to radiation observed in the diseased cells. Although the radiation can be delivered accurately to a tumor in the body, a noticeable pattern has developed where typical doses fail to entirely kill the targeted cells, resulting in a demand for higher radiation levels, putting even more healthy cells at risk [1]. In response to these developments, researchers have proposed radiosensitization to solve the dangers associated with amplified radiation exposure [2,4].

Radiosensitization involves directly infiltrating tumor cells with an agent to alter their susceptibility to the effects of radiation, which in turn allows for lowered radiation dosages, higher cancerous cell death, and more accurate therapeutic targeting [1]. The agents by which this is accomplished are called radiosensitizers, and they can include metal-based nanoparticles, non-metal-based nanoparticles, quantum dots, and superparamagnetic iron oxides [5-8]. Once in the cancerous tissue, these nanoparticles absorb the administered radiation, which releases high-energy electrons, photons, and radicals that interact with water, resulting in fatal damage to the local DNA strands [9]. Therefore, the nanoparticles present in the tumor amplify the effect of the smaller doses of radiation and more effectively harm the cancerous tumor cells while lowering the risk of damage to the surrounding healthy tissue.

Gold Nanoparticles, or GNP, are a specific subset of the metal-based nanoparticles that have been found to display physical and chemical properties optimal for radiosensitization and nuclear imaging [10]. In addition to the GNP's favorable size, they also have an enhanced mass energy absorption coefficient, higher scattering of electromagnetic radiation, fast and convenient manufacture, necessary biocompatibility, and have sufficient binding affinities for biological markers when functionalized with the appropriate ligands [11]. Together with their ability to infiltrate cancerous cells in vivo, these characteristics make these nanoparticles excellent candidates to serve as effective radiosensitizers.

Before the widespread implementation of radiosensitization using GNP can be achieved, it is essential to know precisely where these GNP localize, how long they remain within the body, and the extent to which they harm healthy cells. To conduct these studies in the laboratory and clinical settings, the radiosensitizers must be visible to non-invasive imaging technology. Traditional GNPs are not inherently radioactive and cannot be detected by commonly used clinical nuclear imaging methods such as single-photon emission computed tomography (SPECT) and positron emission tomography (PET). To address imaging issues, radionuclides that emit γ and β^+ are often

attached to the desired molecule since they are easily traceable in SPECT and PET [12]. In this work, the positron-emitting radionuclide ^{64}Cu-doped GNP are developed that allows for radiosensitization. In addition to being able to view and measure these hybrid GNPs in vivo, they must also retain the same radiosensitization and biocompatibility properties of the traditional GNPs, which can be accomplished by comparing the results of cytotoxicity, biodistribution, and pharmacokinetic studies of the two varieties.

The objective of this work was to develop hybrid functionalized GNPs that both serve as potent radiosensitizers and enable tracking using PET/SPECT imaging. These nanoparticles are presumed to have a core-shell structure, where the core is composed of Cu covered with a gold shell. The scope of the work includes developing and characterizing non-radioactive GNPs through transmission electron spectroscopy (TEM), ultraviolet-visible (UV-Vis) spectroscopy, and inductively coupled plasma atomic emission spectroscopy (ICP-AES). The hybrid GNPs were functionalized with varying amounts of cMBP (Lys-Ser-Leu-Ser-Arg-His-Asp-His-Ile-His-His-His), a peptide known to specifically target and bind Mesenchymal-epithelial transition factor (c-Met). The cMBP peptide was first identified from a phage display of a combinatorial peptide library by Kim and his colleagues. [13]. The c-Met is known to overexpress in tumor cells, such as the A-549 human lung cancer cells used in our studies [14]. These functionalized GNPs, when doped with ^{64}Cu (half-life of 12.7 hours), have sufficiently long to measure their binding properties through cell-binding studies [15]. Since the ^{64}Cu doping is achieved in the particle core, which is protected by the gold shell, the risk of the radiolabels detaching from the GNPs is eliminated. The cytotoxicity of the unfunctionalized Cu@Au nanoparticles was determined by measuring cell viability as a function of the concentration of the GNPs. The radiolabeled hybrid GNPs were then administered to mouse and rat models and traced by gamma detection to evaluate their biodistribution and pharmacokinetic properties.

2. Materials and Methods

2.1. Synthesis of functionalized ^{64}Cu@Au GNPs

The GNP production method used in this study was based on the citrate-stabilized synthesis process reported by Zhang and his colleagues. [16]. Briefly, 50 mL of a 0.1 M CuSO4 solution and 150 μL of a 0.1 M sodium citrate solution were added to 20 mL of water at 12 ± 2 °C while stirring at 1,000 rpm. Next, 2 mL of freshly prepared 0.025 M NaBH4 was added to the reaction mixture while stirring, and the stirring was continued for 15 minutes. Then, 150 μL of a 0.1 M aqueous solution of HAuCl4 was added to the reaction mixture and left to stir undisturbed for an additional 20 minutes, resulting in a solution with a rich burgundy hue. The product Cu@Au GNPs were separated from the unreacted salts using gel-filtration. Finally, these GNPs were modified by adding polyethylene glycol (PEG) alone or with cMBP peptide conjugate (cMBP-(PEG2)3-Cys-NH2), which allows the nanoparticles to bind tumor cells as desired. The cMBP-(PEG2)3-Cys-NH2 was synthesized using an in-house built peptide synthesizer and purified by high-performance liquid chromatography (HPLC) [17]. Matrix-assisted laser desorption/ionization (MALDI) mass spectrometry was utilized to characterize the peptide conjugate. Finally, the hybrid Cu@Au GNPs were functionalized by attaching varying amounts of cMBP and PEG, which specifically target the c-Met.

The plans for radiolabeling the GNPs using ^{64}Cu were created according to the guidelines expressed in the ALARA (as low as reasonably achievable) radiation-protection principle in addition to the regulations provided

by the University of Oklahoma Health Sciences Center. To obtain the copper isotope for doping, ^{64}Cu was purchased from the Washington University School of Medicine cyclotron facility. The radiolabeling of the GNPs was conducted in a lead-shielded fume hood where the synthesis process was as described in the synthesis process of core-shell Cu@Au GNPs with the addition of ^{64}Cu-chloride aqueous solution based on the overall function they were to serve in the experiment.

2.2. Characterization of Cu@Au GNPs

UV-vis spectroscopy is utilized to examine the nanoparticles' physical properties that directly influence their optical properties, such as absorption, excitation, and emission peaks, observed in this technique. Using UV-vis spectroscopy, GNPs are identified based on size, shape, concentration, and the index of refraction near their surface. The absorbance peak of the hybrid GNPs was measured using a Cary 5000 Varian UV-vis-NIR spectrophotometer. The color transitions observed are correlated to the size and thickness of the shell in a core-shell structure, which mainly occur in the visible spectrum and describe the size and morphology of particles [18].

TEM uses a focused beam of electrons transmitted through a sample leading to the formation of an image to measure the size, shape, and arrangement of the GNPs by directly imaging them. The samples used were prepared by dropping 2 µL of GNPs onto a carbon-coated copper grid and letting them air dry for four minutes. The grid was then mounted onto the TEM instrument, which was a JEOL, JEM 2100, and different images were obtained exploring various zooming modalities. In interpreting these results, the light areas of the TEM image represent lower density areas of the grid where electrons are more easily passed through. To obtain further information about the Cu@Au GNPs using this technique, TEM was used combined with Energy-Dispersive X-ray Spectroscopy (EDS). Results from EDS describe the elemental composition of a nano-sized area. Both of the TEM and TEM/EDS measurements for this study were recorded at the Oklahoma State University electron microscopy laboratory.

To determine the metal composition of the GNPs, inductively coupled plasma atomic emission spectroscopy (ICP) measurements were carried out at the Oklahoma State University soil, water, and forage analytical lab using Spectro Arcos. These results quantified the metals present in the GNPs and detected Au and Cu over a wide range of concentrations. In further examining the Au in the GNPs, X-ray photoelectron microscopy, XPS, provided information about the nature of Au bonds in addition to surface analysis. The XPS spectra were acquired using the Al-Kα emission line from a dual anode X-ray source (Physical Electronics XR 04-548) operated at 400 W and an incident angle of 54.7° in an ultra-high vacuum system (UHV) with a base pressure of 1.0×10^{-9} Torr.

2.3. Cell Uptake Studies

In vitro cell binding studies were performed to determine the binding affinity of cMBP-GNPs to c-MET expressing cells and the optimal amount of peptide functionalization. In the first method, different peptide-functionalized (0%, 1%, 3%, 5%, 10% functionalization of the estimated Au atoms on the surface) nonradioactive GNPs and the A-549 cells (1×10^6 cells/well) were incubated in a 96-well plate. After 45 minutes, the cells were washed with phosphate-buffered saline, PBS, three times to remove the residual GNPs that did not bind to the

cells. The cells were then digested with NaOH (0.1 M)/SDS (0.1%) and collected and analyzed by ICP to determine the Au/Cu concentrations. Due to insignificant results, the experiment was repeated with 1-hour and 4-hour incubation times. In the second method, the same procedure was followed with radiolabeled GNPs. The same varied peptide concentrations used in the first method were bound to the radiolabeled ^{64}Cu@Au GNPs. Then, an activity of 1 µCi was added to each well, and the cells were incubated for 2 hours before measuring the cell-bound activity using a gamma counter.

2.4. In vitro Cytotoxicity

To determine the cytotoxicity of the hybrid GNPs, A-549 cells were first seeded in a 96-well plate at 3×10^3 cells per well. Then, the cells were cultured in a standard condition in an incubator for 24 hours. Different concentrations of Cu@Au GNPs (1,000, 750, 500, 250, 100, 50, and 25 µg/mL diluted in Roswell Park Memorial Institute, RPMI, medium) were then added to the wells, and the cells were incubated for 48 hours. After that, 3-(4,5-dimethylthiazole-2-yl)-2,5-diphenyl tetrazolium bromide (MTT) 5 mg/mL in PBS was added to each well. Finally, a Synergy 2, Biotec plate reader was used to evaluate the resulting in vitro cell viability and toxicity profile. The viability result for the control cells was set at 100%, and the viability of the treated cells was expressed as a comparison relative to the control. Typically, in toxicity experiments conducted on nanoparticles, 20 µL of MTT is added to each well, followed by a resting time of 2 hours to allow for the absorption of the MTT by the cells. During this process, live cells turn the yellow color of the MTT to blue. Since the hybrid GNPs developed had deep red color, the color shift from yellow to blue, indicating optical absorbance would be obscured. To adjust this issue, instead of adding MTT to the wells, first, the GNPs and medium from the top of each well were carefully removed by using vacuum suction. Then 20 µL of MTT diluted in 100 µL of the medium was added to each well and analyzed. The optical density was read at 570 nm and used to calculate IC_{50}.

2.5. Biodistribution Study

In vivo biodistribution studies were conducted in healthy CD-1 mice, and pharmacokinetics studies were carried out in healthy Sprague Dawley rats, all of which were executed according to the protocol approved by the OUHSC Institutional Animal Care and Use Committee. In the preliminary biodistribution study, the organs and organ systems responsible for the elimination of ^{64}Cu@Au GNPs from the blood were investigated in mice. Different doses of ^{64}Cu@Au GNPs were injected into the tail vein of the mice under isoflurane anesthesia. For each data collection time interval: 1 hour (10 µCi/mouse), 4 hours (15 µCi/mouse), 24 hours (50 µCi/mouse), and 48 hours (100 µCi/mouse). Each group consisted of four mice. At each time point after injection, the designated mice were euthanized by cervical dislocation, and various organs were collected to determine the activity present in the tissue using a well-counter. The activity was normalized to the tissue's weight and presented as the percentage of the injected dose per gram of tissue and subsequently as the percentage of injected dose per organ.

2.6. Pharmacokinetics

Pharmacokinetics studies of ^{64}Cu@Au GNPs were carried out on male Sprague Dawley rats. Rats weighing between 200-225 g are the optimal size for installing an indwelling femoral artery catheter. This catheter can be

used to sample blood at different intervals to determine the clearance rate of ^{64}Cu@Au GNPs. 7 rats were injected with the same dose of 40 µCi, but each injection contained different amounts of ^{64}Cu@Au GNPs. To optimize statistical data, 3 rats were injected with 5[GNPs] while 4 rats were injected with 3[GNPs], where [GNPs] represents the concentration of the gold nanoparticles. The sampled blood of the 7 rats was collected according to the following volumes and time points: 0.1 mL at 2 min, 5 min, 10 min, 20 min, 30 min, 1 h, 2 h, 4 h, 6 h, 0.3 mL at 24 h, and 0.6 mL at 28 h and 48 h. These blood samples were then counted by a Ludlum Measurements Inc, Model 2200 Scaler Ratemeter gamma counter. Next, activity was corrected for both the decay based on the standard counts and withdrawn blood volume and reported in (counts/µL).

3. Results and Discussion

3.1. Characterization of Cu@GNPs

The Cu@Au GNPs were synthesized according to the optimum conditions previously listed in the material and methods section and were promptly characterized. The UV-Vis spectra of three different samples are shown in **Error! Reference source not found.**. The absorbance peak appeared around 526 nm, which is concurrent with the typical absorbance peak of gold. Upon the addition of $HAuCl_4$, the solution turned wine red instantly, which overall agrees with the conclusions of Zhng and his colleagues. [19]. As suggested by them, during the synthesis, the galvanic displacement reaction between $HAuCl_4$ and Cu nanoparticles takes place following the reduction of $HAuCl_4$ by the remaining $NaBH_4$ after the generation of Cu NPs. They also observed the same color change upon the addition of $HAuCl_4$, indicating a rapid growth of the Au shell onto the Cu core of the nanoparticles. In addition, further investigation in their studies showed that the absorbance of $HAuCl_4$ centered at 218 and 293 nm disappeared after the reaction, and a new absorbance band emerged at 520 nm, which is the feature of the gold surface Plasmon resonance SPR. In their experiment, after 24 hours, the new gold SPR band was extended to 530 nm and became a little more intense, displaying a quick growth of Au shell onto the Cu NPs core. This growth could indicate a complete transformation of $AuCl_4$ to clusters of Au atoms with an average size above 2 nm that confirms the color of the synthesized Cu@Au GNPs and UV-Vis spectra obtained from this experiment [16].

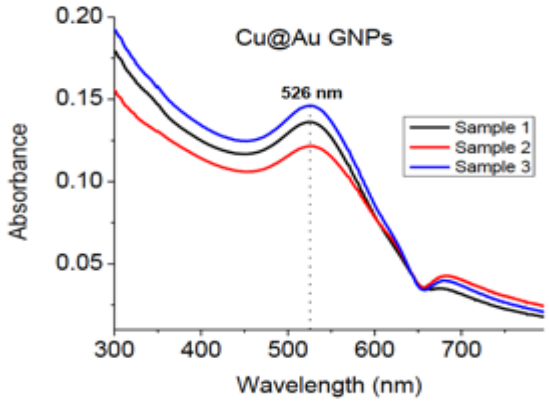

Figure 1: Absorbance peak of Au around 526 nm confirmed by UV-Vis spectrophotometer for different samples

Further, TEM imaging was performed to provide descriptions of the shape, size, and distribution of both stable GNPs and the radiolabeled GNPs after the complete decay of ^{64}Cu. The resulting micrographs show that Cu@Au GNPs 2 hours post-synthesis were more irregular in geometry and more separated with an average size smaller than 10 nm (

Figure **2**a, b). After 24 hours, more regular, spherical particles occurred with a clustered distribution (

Figure **2**c, d).

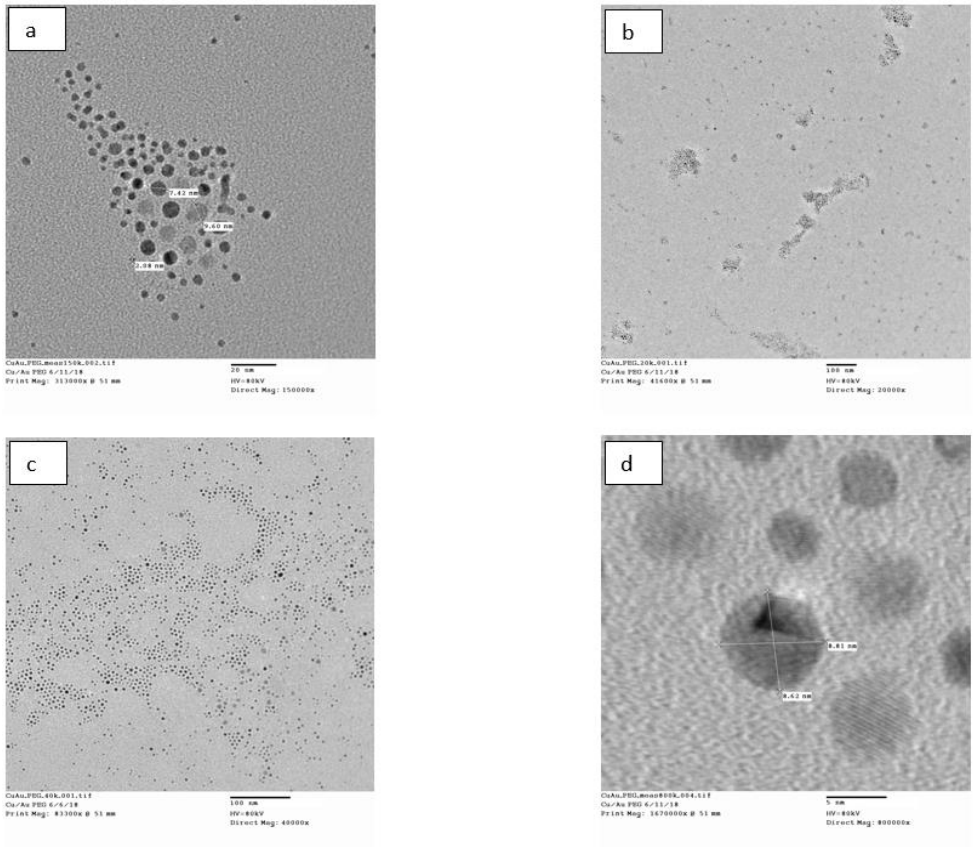

Figure 2: a) TEM on GNPs after 2 h, magnification: 150 K. b) Distribution of GNPs after 2 h, magnification: 20K. c) Distribution of GNPs after 24 h, magnification: 40K. d) GNPs showing the spherical shape after 24 h, magnification: 800 K

The radiolabeled ^{64}Cu@Au GNPs show the same average size, distribution, and morphology as the stable Cu@Au GNPs, as shown in **Error! Reference source not found.**.

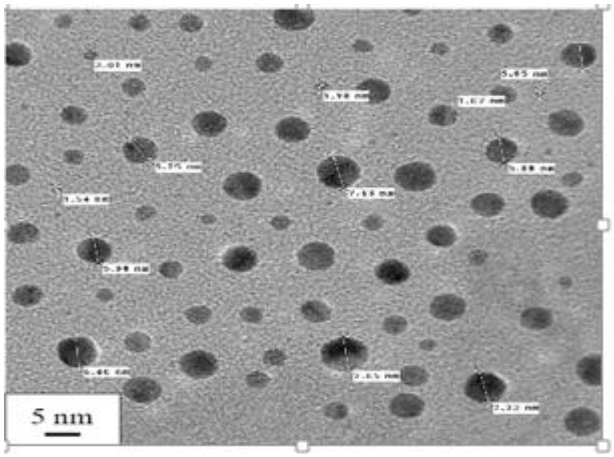

Figure 3: TEM on the radiolabeled GNPs after decay. The average size is less than 10 nm, mag: 250 K

TEM/EDS analysis was performed on different parts of the grid to obtain more detailed information about the copper and gold distribution in the sample. To reduce the effect of Cu's presence in parts of the electron microscope and the grids, a Ni grid was used. The background was subtracted, i.e., a value typically found on empty grids and areas not containing particles. Besides, due to the particles' small size, less than 10 nm in length, and the limitations in magnifying the EDS device used, the measurement from one single particle could not be taken. Therefore, the reported quantities are only from a micrometer-sized area of the grid containing several particles rather than just one particle. The TEM/EDS spectrum from a partial region of the Cu@Au GNP sample is displayed in Figure 4. The result showed the presence of X-ray dispersion energy peaks characteristic of gold (Au(M) ≈ 1.120 keV, Au(Lα) ≈ 9.712 keV) in addition to less intense characteristic X-ray dispersion energy peaks of copper (Cu(Lα) ≈ 1.00 keV, Cu(Kα) ≈ 8.00 keV). These results are similar to the results of EDS analysis of nanoparticles containing Au and Cu reported in the literature [20,22].

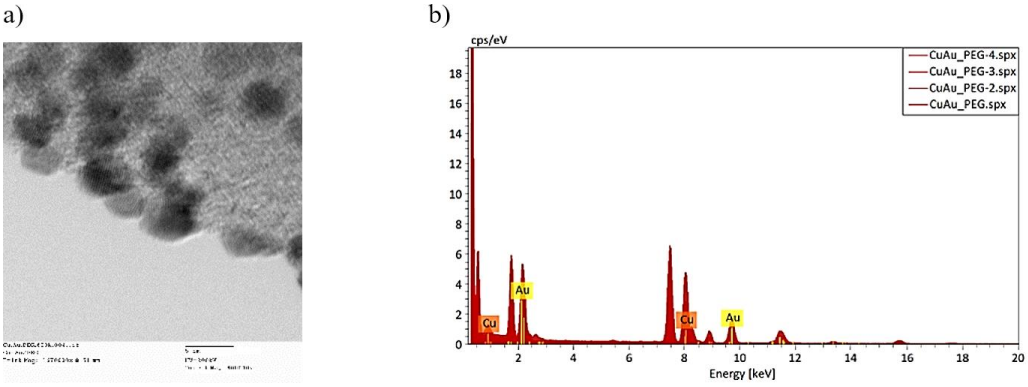

Figure 4: a) TEM and b) EDS analysis of Cu@Au GNPs on a micrometer-sized area of a nickel grid

The values of Au and Cu present in the micrometer-sized area of the grid were measured several times from different parts of the grid, and the average is shown in Table 1.

Table 1: The average percentage of Au and Cu present in the micrometer-sized area of the grid

Cu@Au GNPs/PEG	Gold	Copper
Average	23.57%	76.43%

The XPS analysis can be used to confirm the core/shell structure of the GNPs with a good approximation. As seen in Figure 5a, Au 4f XPS core level spectrum exhibits a peak for Au $4f_{7/2}$ located at binding energy, E_B, of 84.3 eV with a well-separated spin-orbit component (Δ=3.7eV), which is consistent with the metallic gold atom binding energy (Au^0, E_B = 84.0 eV). The shift of binding energy for Au $4f_{7/2}$ compared to that of zero-valance gold atom, 84.0 eV, could be due to an electronic modification of the Au atoms by Cu NPs [16,23]. Figure 5b shows the XPS spectrum of Cu 2p core level. The E_B for Cu $2p_{3/2}$ peak is 933.3 eV. Cu2p peak has a significant spin-orbit split component (Δ=19.75 eV), which is consistent with Cu^0 and Cu(I) oxide (E_B=933.0 eV). This observation shows that the majority of Au and Cu present in the nanoparticles are in their zero-valence state [24]. The database used to compare the binding energies are taken from https://xpssimplified.com/periodictable.php.

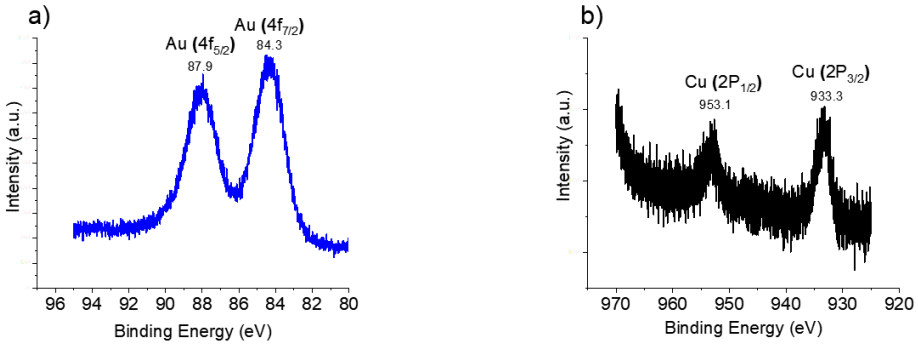

Figure 5: XPS core-level spectra for a) Au 4f and b) Cu 2p in Cu@Au GNPs

Table 2 represents the ICP results for several samples used in this study. The ratio of Au:Cu is in the range of 7.6-11.5. Based on the numeric result obtained from ICP, more than 50% of the initial Au and more than 90% of the initial Cu were used in the reaction. This result is solely based on the assumption that Au atoms are all in the shell and by calculating the approximate number of Au atoms on the surface from the average particle size and the atomic radius of gold.

Table 2: ICP results of a variety of samples used in this study

Material	Au (ppm)	Cu (ppm)	Au (µg/ml)	Cu (µg/ml)	Au/Cu ratio
GNP before passing through size-exclusion column	11.60	1.53	116.0	15.3	7.6
Colored GNP after passing through size-exclusion column	3.76	0.42	37.6	4.2	9.0
GNP used for PK studies, 5X concentration	4.06	0.38	13.5	1.3	10.8
GNP used for PK studies, 3X concentration	8.27	0.82	82.7	8.2	10.1
GNP used for cytotoxicity	11.96	1.04	1495.1	129.5	11.5
GNP evaporated and filtered for targeting	14.18	1.49	1418.0	148.7	9.5

3.2. Cell Uptake Studies

The result of ICP for digested cells after 1-h and 4-h incubation times with functionalized GNPs did not show any significant trace of Au and Cu, indicating that no uptake had occurred. This can be due to several factors ruling the cell uptake. Among all reasons, the most trivial ones are peptides not binding to the GNPs, and c-Met expression not being well defined on the A549 cells. Targeting the cells with radiolabeled GNPs did not yield any meaningful cell uptake results either. Hence, it was decided to perform the cytotoxicity studies with unfunctionalized GNPs (Cu@Au GNPs).

3.3. In Vitro Cytotoxicity of Cu@Au GNPs

The plot of the A-549 cell viability and the concentration of the Cu@Au GNPs obtained from this study's results is seen in Figure 6. Each point represents the average viability of up to six wells for each concentration. The curve fitted to the data points was used to determine the half-maximal inhibitory concentration (IC_{50}), which is the concentration of the GNPs at which the viability of the cells reached 50% of the maximum viability. This was calculated according to the following equation: maximal viability – 50%(maximal viability – minimal viability) Reference [25]. The IC50 value for the hybrid Cu@Au GNPs was found to be 807.2 ± 0.05 µg/mL, which is within the reported range of 500-12,00 µg/mL found in the literature for nanoparticles less than 15 nm in size for various types cell types [26,27].

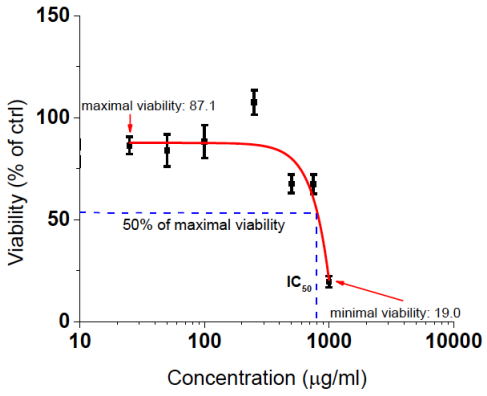

Figure 6: The cell viability was calculated as the average percentage of the viable cells for each concentration of the control cells' viability where viability was measured using MTT assay

3.4. In Vivo Biodistribution of ^{64}Cu@Au GNPs in Mice

The biological pathways responsible for the uptake and clearance of the ^{64}Cu@Au GNPs were identified through biodistribution studies. Figure 7 shows the accumulation of the GNPs in various organs and tissue of the mice after 1 hour, 4 hours, 24 hours, and 48 hours. At all-time points, the liver and the intestines displayed the largest percentage of the injected dose significantly determined by the samples' gamma emissions. Therefore, it is inferred

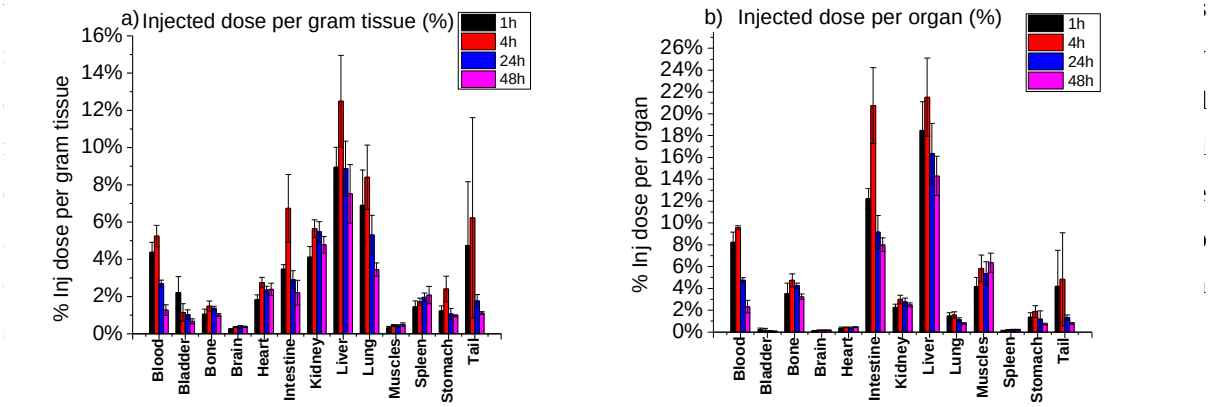

Figure 7: The average biodistribution results of ^{64}Cu@Au GNPs in sixteen mice—4 for each time interval. 7a shows the percentage of the injected dose per gram of tissue measured, while 7b shows the percentage of injected dose per organ

3.5. In Vivo Pharmacokinetics of ^{64}Cu@Au GNPs in Rats

The seven rats used were randomly divided into a group of 3 and a group of 4. The former group received injections with a 5X concentration of ^{64}Cu@Au GNPs, while the latter received a 3X concentration of ^{64}Cu@Au GNPs. The pharmacokinetics values were calculated based on the average data measured for each group. In this study, the pharmacokinetic data measured included the area under the concentration vs. time curves from where time = 0 to time = ∞ ($AUC_{0-\infty}$) and the area under the first moment curve (AUMC). Maximum GNP concentration (C_{max}) was determined directly from the concentration vs. time plot. The Mean Residence Time (MRT), the average time that the GNPs remain in the body, was calculated by dividing AUMC by AUC. The Total Clearance (Cl) value was calculated as the dose/$AUC_{0-\infty}$. The average decay-corrected injected dose is 40 µCi. In addition, the volume of distribution at a steady-state (Vss) was calculated as MRT×Cl, and the apparent elimination rate constant ($kel^{'}$) was calculated as 1/MRT. Finally, elimination half-life ($t_{1/2}$) represented the amount of time required for the amount of drug in the body to decrease by 50% and was found to be $t_{1/2}$= 0.693/ $kel^{'}$. The concentration vs. time curves for each group are shown in Figure 8.

The $AUC_{0-\infty}$ was calculated using the AUC_{0-last} and then extrapolating to infinity by the addition of $AUC_{last-\infty}$, given as $\frac{C_{last}}{\lambda}$, shown in the equation below. The graph from which AUC_{0-last} (total AUC) is calculated is presented in Figure 9.

$$AUC_{0-\infty} = AUC_{0-last} + \frac{C_{last}}{\lambda} \quad (1)$$

Where λ is the terminal slope from a semi-log concentration-time graph as seen in Figure 10.

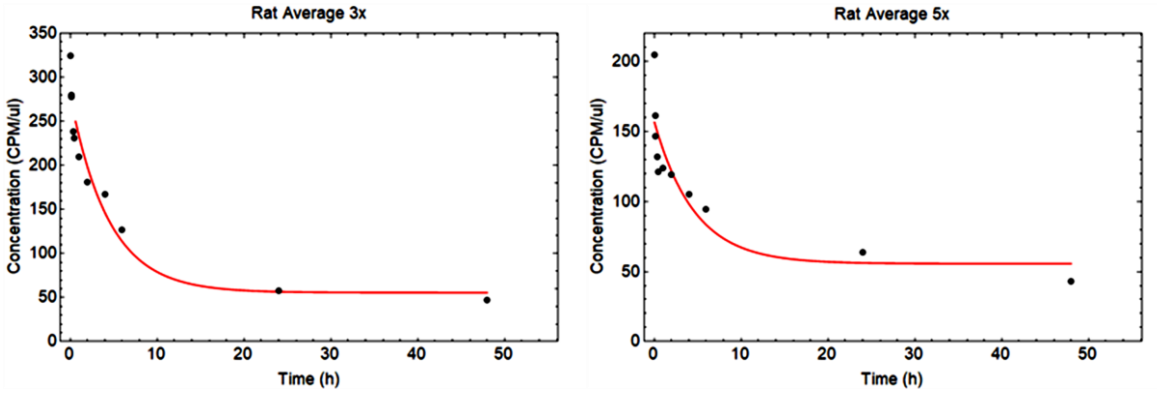

Figure 8: The concentration vs. time curves for the average data for two concentrations of ^{64}Cu@Au GNPs with a constant activity where the red lines represent the curves fitted to the data

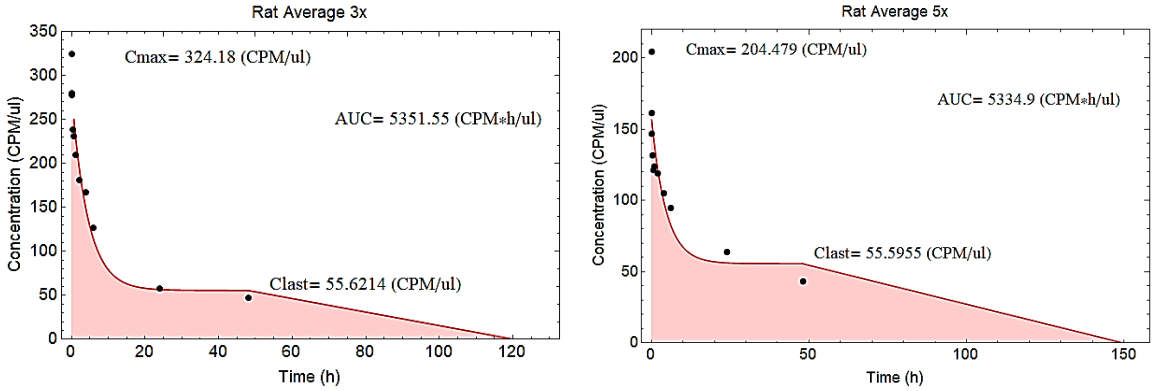

Figure 9: Total AUC (AUC0–last) represented by the pink area after the fitted curve was extrapolated to infinity using λ

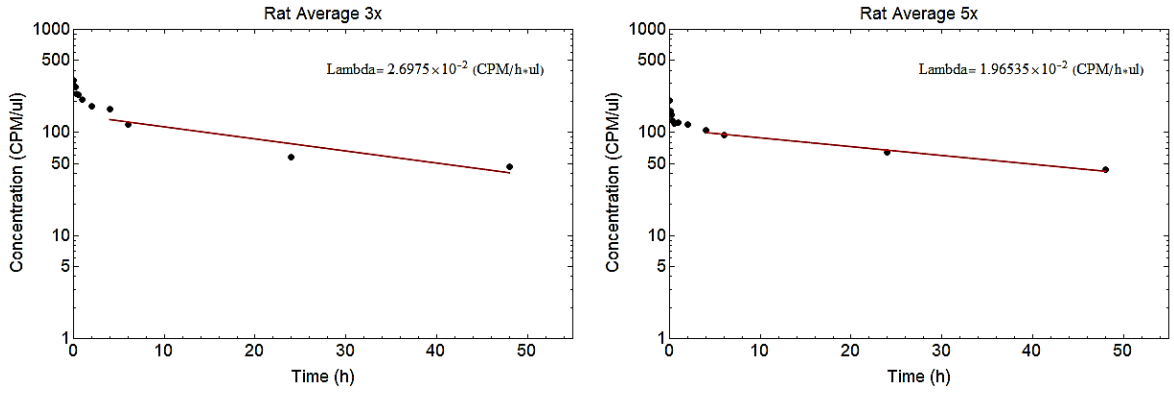

Figure 10: The semi-log plot of concentration vs. time to find the terminal slope

Figure 11 represents the first moment of the data, represented by the area under the "concentration×time – time" curve (AUMC), and the fitted plot. The following equation shows the method used to extrapolate the curve, and its representation is shown in the shaded region in (Figure 12).

$$\boldsymbol{AUMC_{0-\infty} = AUMC_{0-last} + \frac{C_{last} \cdot t_{last}}{\lambda} + \frac{C_{last}}{\lambda^2}} \quad (2)$$

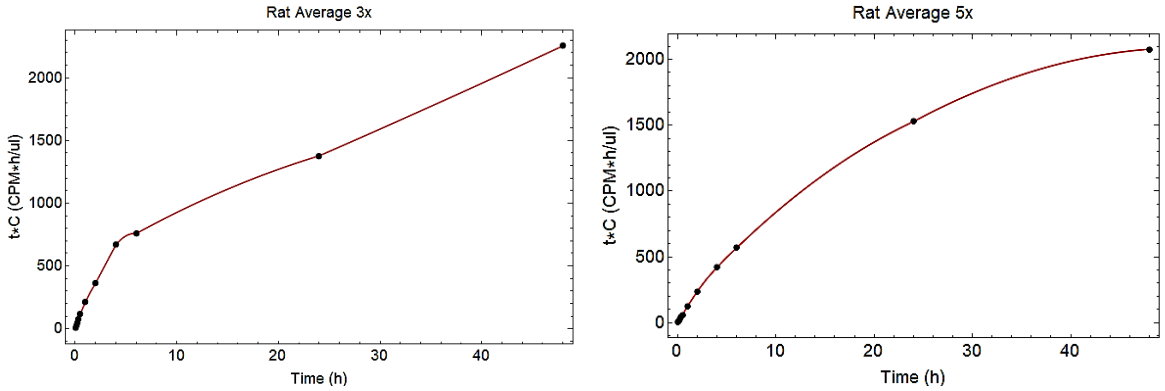

Figure 11: The first moment of the data: the plot of the concentration×time vs. time. The data were fitted as shown by the red line

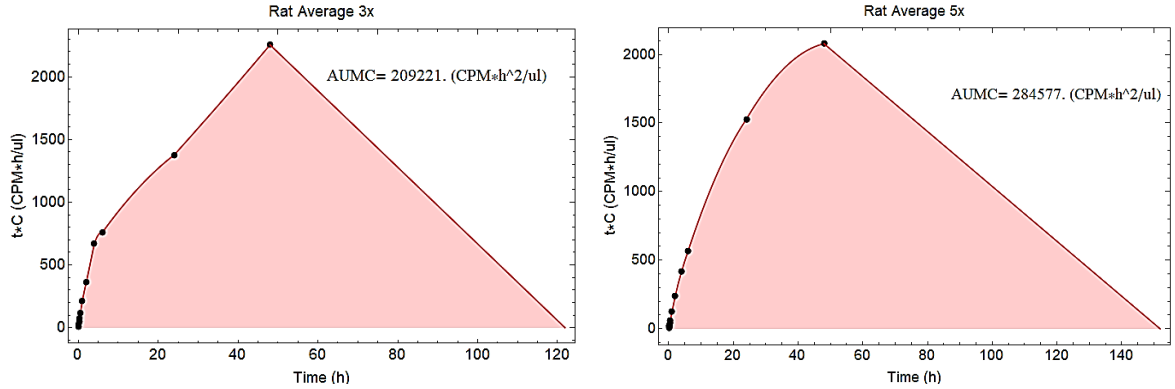

Figure 12: The AUMC extrapolated to infinity using λ. The shaded area represents the total area under the curve ($\boldsymbol{AUMC_{0-\infty}}$)

Table 3 summarizes the pharmacokinetic parameters that were calculated.

Based on the result provided below, the clearance rate of different concentrations of ^{64}Cu@Au GNPs is similar with a good approximation (~ 1.9 ml/h). The mean volume of distribution at steady-state, Vss, was higher with the higher concentration of the particles (~99.7 ml) than the 3X concentration (~72.8 ml). The half-life of ^{64}Cu@Au GNPs was also calculated to be about 23 h for 3X and about 35 h 5X concentrations, respectively. As expected, the clearance rate of ^{64}Cu@Au GNPs is comparable to the rate of 13 nm-sized PEG-coated GNPs, ^{64}Cu@CuS NPs, and solid lipid NPs [28,30].

Table 3: The pharmacokinetic parameters calculated in these studies

PK Parameters	^{64}Cu@Au GNPs (3X)	^{64}Cu@Au GNPs (5X)
$AUC_{0-\infty}$ (CPM.h/µl)	5,351.6	5,334.9
$AUMC_{0-\infty}$ (CPM.h^2/µl)	209,221	284,577
Cmax (CPM/ µl)	324.2	204.8
MRT (h)	39.1	53.3
Cl (µl/h)	1,862.3	1,868.1
Vss (µl)	72,798.9	99,647.1
Kel' (1/h)	0.03	0.02
$t_{1/2}$ (h)	23.1	34.6

4. Conclusion

The results from UV-vis spectrophotometry, TEM, TEM/EDS, XPS, and ICP confirm that non-radioactive Cu@Au GNPs were developed. The Cu@Au GNPs were then functionalized with varying amounts of cMBP to target c-Met receptors expressed on A-549 human lung cancer cells. The results of ICP for digested cells after 1- and 4-hour incubation with the functionalized GNPs indicated that no uptake had occurred. This can be due to multiple factors ruling the cell uptake. The most trivial reasons are peptides not binding to the GNPs, and c-Met expression not being well defined on the A549 cells. Next, the Cu@Au GNPs were doped by ^{64}Cu, creating radiolabeled ^{64}Cu@Au GNPs, which failed to successfully target cells as shown by no cell uptake. In analyzing the toxicity of Cu@Au GNPs in A-549 cells, the IC_{50} of the Cu@Au GNPs was calculated to be 807.2 ± 0.05 µg/ml, which is within the expected range of values of traditional GNPs and similarly sized NPs, indicating comparable biocompatibility. Overall, our findings supported by the results from both the biodistribution studies in mice and pharmacokinetics studies in rats, confirm that although radiolabeled ^{64}Cu@Au GNPs failed to target cells successfully, the non-radiolabeled Cu@Au GNPs have similar physical and biological properties as similarly sized traditional GNPs, leaving room for future studies to overcome the limitations of functionalizing and doping ^{64}Cu with Cu@Au GNPs.

Acknowledgements

S.B. acknowledges Dr. Jongmin Cho for coming up with the basic idea, suggesting the study, and useful discussion. S.B. also acknowledges Dr. V. Awasthi and Dr. Gali at the University of Oklahoma Health Sciences Center (OUHSC) for their assistance and support specially during working with radioactivity. She also acknowledges Dr. David McIlroy for valuable discussions about this work and for offering the use of the XPS system for characterization. Moreover, S.B. acknowledges Ms. Hedrick, Dr. Mdzinarishvili, Dr. Nkepang, Dr. Pathuri, and Dr. Yari for helping her perform all the in vitro and in vivo studies.

References

[1] D. Kwatra, A. Venugopal, and S. Anant, "Nanoparticles in radiation therapy: a summary of various

approaches to enhance radiosensitization in cancer," Transl. Cancer Res., vol. 2, no. 4, pp. 330–342, 2013.

[2] R. Schürmann, S. Vogel, K. Ebel, and I. Bald, "The Physico-Chemical Basis of DNA Radiosensitization: Implications for Cancer Radiation Therapy," Chem. Eur. J., vol. 24, no. 41, pp. 10271–10279, 2018.

[3] P. Maier, L. Hartmann, F. Wenz, and C. Herskind, "Cellular pathways in response to ionizing radiation and their targetability for tumor radiosensitization," *Int. J. Mol. Sci.*, vol. 17, no. 1, p. 102, 2016.

[4] A. Deorukhkar and S. Krishnan, "Targeting inflammatory pathways for tumor radiosensitization," *Biochem. Pharmacol.*, vol. 80, no. 12, pp. 1904–1914, 2010.

[5] X.-Y. Su, P.-D. Liu, H. Wu, and N. Gu, "Enhancement of radiosensitization by metal-based nanoparticles in cancer radiation therapy," *Cancer Biol. Med.*, vol. 11, no. 2, pp. 86–91, Jun. 2014, doi: 10.7497/j.issn.2095-3941.2014.02.003.

[6] S. Klein *et al.*, "Oxidized silicon nanoparticles for radiosensitization of cancer and tissue cells," *Biochem. Biophys. Res. Commun.*, vol. 434, no. 2, pp. 217–222, May 2013, doi: 10.1016/j.bbrc.2013.03.042.

[7] P. Juzenas *et al.*, "Quantum dots and nanoparticles for photodynamic and radiation therapies of cancer," *2008 Ed. Collect.*, vol. 60, no. 15, pp. 1600–1614, Dec. 2008, doi: 10.1016/j.addr.2008.08.004.

[8] G. Huang *et al.*, "Superparamagnetic iron oxide nanoparticles: amplifying ROS stress to improve anticancer drug efficacy," *Theranostics*, vol. 3, no. 2, pp. 116–126, 2013, doi: 10.7150/thno.5411.

[9] J. D. Carter, N. N. Cheng, Y. Qu, G. D. Suarez, and T. Guo, "Nanoscale Energy Deposition by X-ray Absorbing Nanostructures," *J. Phys. Chem. B*, vol. 111, no. 40, pp. 11622–11625, Oct. 2007, doi: 10.1021/jp075253u.

[10] B. Jeremic, A. R. Aguerri, and N. Filipovic, "Radiosensitization by gold nanoparticles," *Clin. Transl. Oncol.*, vol. 15, no. 8, pp. 593–601, Aug. 2013, doi: 10.1007/s12094-013-1003-7.

[11] P. K. Jain, K. S. Lee, I. H. El-Sayed, and M. A. El-Sayed, "Calculated Absorption and Scattering Properties of Gold Nanoparticles of Different Size, Shape, and Composition: Applications in Biological Imaging and Biomedicine," *J. Phys. Chem. B*, vol. 110, no. 14, pp. 7238–7248, 2006, doi: 10.1021/jp057170o.

[12] J. S. Welsh, "Beta Radiation," *The Oncologist*, vol. 11, no. 2, pp. 181–183, Feb. 2006, doi: 10.1634/theoncologist.11-2-181.

[13] K. Kim et al., "A neutralizable epitope is induced on HGF upon its interaction with its receptor cMet," Biochemical and biophysical research communications, vol. 354, no. 1, pp. 115-121, 2007

[14] J. G. Christensen, J. Burrows, and R. Salgia, "c-Met as a target for human cancer and characterization of inhibitors for therapeutic intervention," *Cancer Lett.*, vol. 225, no. 1, pp. 1–26, 2005, doi: 10.1016/j.canlet.2004.09.044.

[15] C. J. Anderson and R. Ferdani, "Copper-64 radiopharmaceuticals for PET imaging of cancer: advances in preclinical and clinical research," *Cancer Biother. Radiopharm.*, vol. 24, no. 4, pp. 379–393, Aug. 2009, doi: 10.1089/cbr.2009.0674.

[16] J. Zhang, X. Xu, C. Yang, F. Yang, and X. Yang, "Colorimetric Iodide Recognition and Sensing by Citrate-Stabilized Core/Shell Cu@Au Nanoparticles," *Anal. Chem. Wash.*, vol. 83, no. 10, pp. 3911–3917, 2011, doi: 10.1021/ac200480r.

[17] "Reports from University of Oklahoma Health Sciences Center Highlight Recent Findings in Science (An Open-Source Automated Peptide Synthesizer Based on Arduino and Python)," *Sci. Lett.*, p. 2482, Apr. 2017.

[18] J. W. L. Eccles, U. Bangert, M. Bromfield, P. Christian, A. J. Harvey, and P. Thomas, "UV-Vis plasmon studies of metal nanoparticles," *J. Phys. Conf. Ser.*, vol. 241, p. 012090, 2010, doi: 10.1088/1742-6596/241/1/012090.

[19] X.-D. Zhang *et al.*, "Size-dependent in vivo toxicity of PEG-coated gold nanoparticles," *Int. J. Nanomedicine*, vol. 6, pp. 2071–2081, 2011, doi: 10.2147/ijn.s21657.

[20] F. F. A. C. Silva, "Gallium compounds for the design of (nano)radiopharmaceuticals," Ph.D. Thesis, AA(Universidade de Lisboa (Portugal)), 2014.

[21] A. Chu, J. Cook, R. J. R. Heesom, J. L. Hutchison, M. L. H. Green, and J. Sloan, "Filling of Carbon Nanotubes with Silver, Gold, and Gold Chloride," *Chem. Mater.*, vol. 8, no. 12, pp. 2751–2754, Jan. 1996, doi: 10.1021/cm960246w.

[22] K. Rokosz *et al.*, "SEM, EDS and XPS Analysis of the Coatings Obtained on Titanium after Plasma Electrolytic Oxidation in Electrolytes Containing Copper Nitrate," *Materials*, vol. 9, Apr. 2016, doi: 10.3390/ma9050318.

[23] B. G. Bravo, S. L. Michelhaugh, M. P. Soriaga, I. Villegas, D. W. Suggs, and J. L. Stickney, "Anodic underpotential deposition and cathodic stripping of iodine at polycrystalline and single-crystal gold: studies by LEED, AES, XPS, and electrochemistry," *J. Phys. Chem.*, vol. 95, no. 13, pp. 5245–5249, Jun. 1991, doi: 10.1021/j100166a060.

[24] M. Tominaga, Y. Taema, and I. Taniguchi, "Electrocatalytic glucose oxidation at bimetallic gold–copper nanoparticle-modified carbon electrodes in alkaline solution," *J. Electroanal. Chem.*, vol. 624, pp. 1–8, Dec. 2008, doi: 10.1016/j.jelechem.2008.07.005.

[25] M. Stewart and I. Watson, "Standard units for expressing drug concentrations in biological fluids," *Br. J. Clin. Pharmacol.*, vol. 16, no. 1, pp. 3–7, 1983, doi: 10.1111/j.1365-2125.1983.tb02136.x.

[26] V. Kumar and S. Ganesan, "Gold Nanoparticles as an HIV Entry Inhibitor," *Curr. HIV Res.*, vol. 10, Aug. 2012, doi: 10.2174/157016212803901383.

[27] R. Chakravarty *et al.*, "Industrial-Scale Synthesis of Intrinsically Radiolabeled 64CuS Nanoparticles for Use in Positron Emission Tomography (PET) Imaging of Cancer," *Ind. Eng. Chem. Res.*, vol. 55, no. 48, pp. 12407–12419, 2016, doi: 10.1021/acs.iecr.6b03405.

[28] W.-S. Cho *et al.*, "Acute toxicity and pharmacokinetics of 13 nm-sized PEG-coated gold nanoparticles," *Toxicol. Appl. Pharmacol.*, vol. 236, no. 1, pp. 16–24, Apr. 2009, doi: 10.1016/j.taap.2008.12.023.

[29] M. Zhou *et al.*, "A Chelator-Free Multifunctional [64Cu]CuS Nanoparticle Platform for Simultaneous Micro-PET/CT Imaging and Photothermal Ablation Therapy," *J. Am. Chem. Soc.*, vol. 132, no. 43, pp. 15351–15358, Nov. 2010, doi: 10.1021/ja106855m.

[30] H. Dang *et al.*, "Luteolin-loaded solid lipid nanoparticles synthesis, characterization, & improvement of bioavailability, pharmacokinetics in vitro and vivo studies," *J. Nanoparticle Res.*, vol. 16, no. 4, p. 2347, Mar. 2014, doi: 10.1007/s11051-014-2347-9.